

Flower shaped homocentric pencil like ZnO nanorod bundles: synthesis, characterisation and study of their photocatalytic activity†

Cite this: *RSC Adv.*, 2014, 4, 8256

Received 14th October 2013
Accepted 2nd December 2013

DOI: 10.1039/c3ra45818k

www.rsc.org/advances

Diganta Bhuyan,^a Banajit Malakar,^a Sudhir S. Arbuji^b and Lakshi Saikia^{*a}

Flower shaped homocentric pencil like ZnO nanorod bundles are synthesized by a hydrothermal method. The PXRD pattern corresponds to the typical wurtzite structures of ZnO, which exhibits excellent activity as a photocatalyst for the degradation of malachite green under solar light irradiation.

Control of the morphology and size of particulate materials have received more attention recently due to the fact that they play very important roles in determining magnetic, optical, electrical and other properties.¹ One-dimensional nanostructures such as nanowires, nanotubes, nanobelts, and nanorods have attracted great interest because of their novel physical properties as well as their potential applications in constructing nanoscale electronic and optoelectronic devices.² The wide direct band gap (~3.37 eV) and large exciton binding energy (~60 meV) make ZnO an excellent optoelectronic material.³ ZnO has also been confirmed as a promising functional material in other nano-devices such as field emitters⁴ and gas sensors.⁵ The synthesis of ZnO nanostructures is therefore currently attracting intense worldwide interest. Numerous ZnO nanostructures have been demonstrated, for example, nanowires,⁶ nanotubes,⁷ nanobelts,⁸ nanopropellers,⁹ and nanocages.¹⁰ A variety of methods have been employed for the synthesis of ZnO nanomaterials such as high-temperature metalorganic chemical vapor deposition (MOCVD) and thermal evaporation processes.¹¹ These processes require either a high vacuum and temperature or some catalysts. Other methods generally applied to synthesize ZnO nanostructures include electrochemical deposition techniques,¹² hydrothermal methods,¹³ sputter deposition techniques¹⁴ and carbothermal reduction methods.¹⁵ However, these methods generally require harsh reaction conditions, such as high

temperature or accurate gas concentration, flow rate or costly raw materials, or a complex process, and so on. It is therefore important to have a simple, cost effective and low temperature method for the synthesis of ZnO nanomaterials.

Herein, the flower shaped homocentric pencil like ZnO nanorod bundles were synthesized using the procedure employed for the synthesis of nanotubes, taking PEG-4000 as a template at a pH of about 9.7. The hydrothermal reaction was carried out at 110 °C in a Teflon lined steel autoclave for 16 h.

The PXRD pattern of the ZnO flowers is shown in Fig. 1. All diffraction peaks can be indexed as a wurtzite structure of ZnO (JCPDS 36-1451, $a = 3.24982$ Å, $c = 5.20661$ Å). No peak attributable to possible impurities is observed. The sharp diffraction peaks indicate that the as-synthesized ZnO nanostructure has high crystallinity. The intensity of the ZnO (002) peak is much stronger than that of bulk ZnO, revealing [0001] growth orientation of the ZnO flowers and indicating that the synthesized ZnO is a 1D structure.

The wurtzite-structured ZnO crystal is described schematically as a number of alternating planes composed of tetrahedrally coordinated O²⁻ and Zn²⁺ ions, stacked alternately along the c -axis. The oppositely charged ions produce positively charged (0001)-Zn and negatively charged (000 $\bar{1}$)-O polar

^aMaterials Science Division CSIR-North East Institute of Science and Technology, Jorhat-785006, Assam, India. E-mail: lakshi_saikia@yahoo.com

^bCentre for Materials for Electronics Technology, Off Pashan Road, Panchwati, Pune-411008, India

† Electronic supplementary information (ESI) available: Synthesis procedure, PL, FT-IR and UV-Vis spectra. See DOI: 10.1039/c3ra45818k

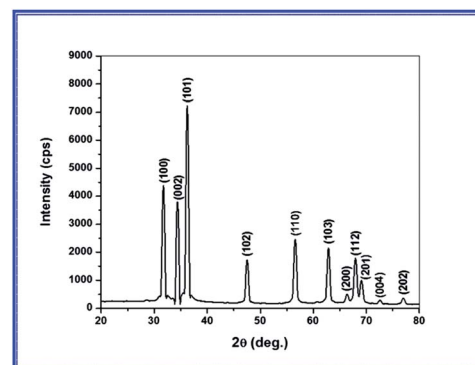


Fig. 1 PXRD pattern of the as-synthesized ZnO flowers.

surfaces,¹⁶ and the Zn-terminated Zn-(0001) polar surface is chemically active whether the oxygen-terminated (000 $\bar{1}$) polar surface is inert or not.¹⁷ In this report, the formation of nanorods may be due to the seed growth of ZnO nuclei on the rod shaped PEG micelle, and the sharp pencil like tip was developed because PEG micelles were attached to the nonpolar faces of the hexagonal ZnO nanocrystal, which allowed growth of the nanorod only along the [0001] direction (Scheme S2 & S3, ESI†). Subsequently, as time goes on, the non polar–non polar interaction dominates between the surface attached PEG, so that the ZnO nanorods are aggregated and form nanorod bundles. These ZnO nanorod bundles then grow in several [0001] directions forming a homocentric flower like structure after 16 h of hydrothermal treatment.

Fig. 2A–C show the FESEM images of the synthesized ZnO. Flower-like clusters grow in several directions and have symmetrical arms in level directions. Every arm consists of a few nanorods with almost uniform diameters and an average length of about 3 μm . Fig. 2B shows that the nanorod bundles are highly disperse within the space, without any aggregation between them, and have approximately uniform morphologies with diameters of 250–300 nm and lengths up to 2 μm .

Fig. 2C shows that the ZnO flower is composed of symmetrical nanorod bundles extending radially from the centre. Every rod has a sharp pencil like tip, in comparison with its base, and a length of up to 2 μm . Fig. 2D shows the TEM image of ZnO in an individual nanorod bundle, which suggests that the inner part of the rods are not hollow and that the tip is sharp. Fig. 2A & B shows the FESEM images of ZnO nanorod bundle growth after 8 h hydrothermal treatment and Fig. 2C shows the FESEM image of the ZnO nanorod bundles arranged in a flowery pattern after 16 h of hydrothermal treatment. It can therefore be observed, from the FESEM images, that 16 h of hydrothermal treatment is the optimal time required for the growth of ZnO nanorod bundles to arrange in a flowery pattern.

The formation of ZnO nanorod bundles is mainly affected by the particular hydrothermal temperature, basic pH and micelle

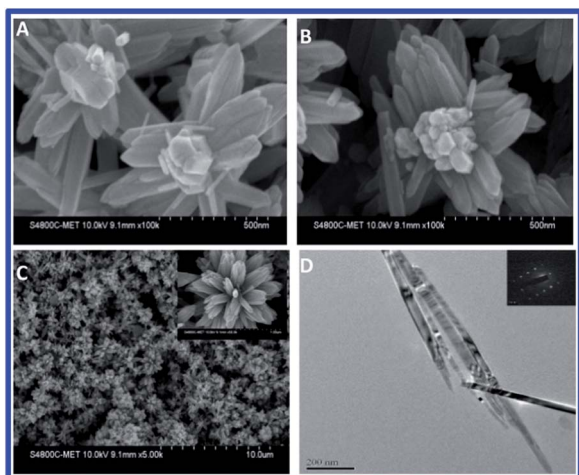


Fig. 2 (A & B) Growth of ZnO flowers (8 h), (C) ZnO flowers (16 h) and (D) TEM image of ZnO in an individual nanorod bundle.

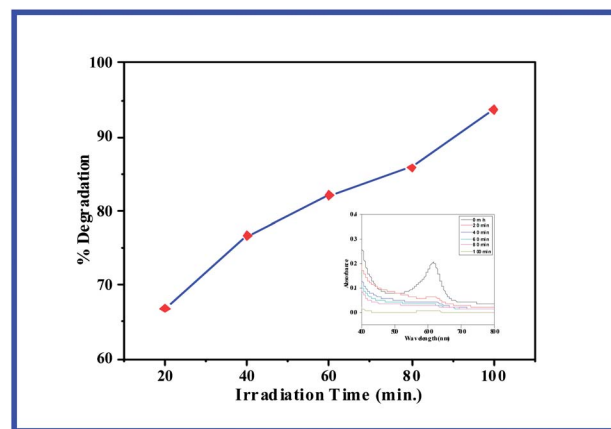


Fig. 3 Photodegradation of malachite green using ZnO flowers as a photocatalyst.

structure PEG-4000 in this report. The ZnO nuclei are obtained by the dehydration of either $\text{Zn}(\text{OH})_4^{2-}$ or $\text{Zn}(\text{NH}_3)_4^{2+}$ in the presence of NH_3 (Scheme S1, ESI†). On the other hand, in the presence of PEG-4000, the growth units $\text{Zn}(\text{OH})_4^{2-}$ or $\text{Zn}(\text{NH}_3)_4^{2+}$ are easily adsorbed by the O atom in the C–O–C chain, so that $\text{Zn}(\text{OH})_4^{2-}$ or $\text{Zn}(\text{NH}_3)_4^{2+}$ can be carried and transformed into ZnO crystalline particles and grow on active sites around the surface of the ZnO nuclei. At a temperature of about 80 $^\circ\text{C}$, a greater amount of NH_3 is produced and Zn^{2+} is transformed into ZnO nuclei at a very fast crystal growth rate. Thus ZnO nuclei aggregate spontaneously with hexagonal symmetry, which provides a chance for the formation of ZnO nanorod bundles. The formation of ZnO is also dependent on pH. When the concentration of ammonia in the system is low (less than $\text{pH} = 9.7$), more $\text{Zn}(\text{NH}_3)_4^{2+}$ are easily transformed into ZnO in the function of weak OH^- . Therefore, abundant ZnO nuclei are formed in the initial stages, which is a possible reason for the formation of some shorter nanorods. There are more EO groups in PEG-4000 than PEG-2000, so more $\text{Zn}(\text{OH})_4^{2-}$ or $\text{Zn}(\text{NH}_3)_4^{2+}$ growth units were adsorbed by the O atom in the C–O–C chain of PEG-4000 and the fast crystal growth rate of ZnO resulted in the formation of ZnO nanorod bundles rather than ZnO nanotubes. PEG-4000 is therefore used as a template for the synthesis of ZnO nanorod bundles; it is shown in Fig. S3 of ESI† that PEG micelles are attached to the non-polar facet of the ZnO crystal which allows for the growth of individual ZnO nanorods in the (0001) polar direction. Due to the hydrophobic interaction existing between these surface attached PEG micelles, the individual ZnO nanorods aggregate and form nanorod bundles after 8 h of hydrothermal treatment. After 16 h of hydrothermal treatment, these ZnO nanorod bundles aggregate at the bottom in a flower like pattern. This is due to the hydrophobic interactions between the surface attached PEG in individual ZnO nanorod bundles, which arranges in a flower like shape due to the same hydrophobic interactions. The growth is therefore unidirectional and attachment occurs at the bottom.

The room temperature photoluminescence spectra have a strong UV emission of 390 nm, a weak blue emission of 468 nm and a broad green-yellow emission of 550 nm (Fig. S1, ESI†). The

green emission at 550 nm originates from the deep level (DL) defect emission associated with oxygen vacancies in ZnO lattices.¹⁸ The blue emission may be from zinc ion vacancies and interstitial zinc defects.¹⁹ The green-yellow emission is stronger in comparison with the blue emission. FTIR spectra of the as-synthesized ZnO flowers have broad bands around 3429 cm⁻¹ and 1589 cm⁻¹, which are due to the surface adsorbed O–H stretching and bending mode of the vibration respectively (Fig. S2, ESI†). The sharp band at 419 cm⁻¹ is a characteristic vibration mode of Zn–O bonding. The UV-Visible spectra of the ZnO flowers have a UV absorption peak at 388 nm and a very broad visible absorption peak (Fig. S3, ESI†). The Brunauer–Emmett–Teller (BET) specific surface area of the material measured by a N₂ adsorption–desorption technique is 26.94 m² g⁻¹, with a hysteresis loop of type IV isotherm (Fig. S4, ESI†) revealing the existence of mesopores in the architecture. The corresponding pore diameter distribution curves (inset in Fig. S4†) show that the size of the mesopores is not uniform but hierarchically distributed, and we mainly attribute the larger size of the mesopores to the explosive release of CO₂ in the confined space of the smaller mesopores during the thermal process. It is reasonable that the release of CO₂ and the collapse of the interconnected mesopores enlarge and change the smaller mesopores into the irregularly shaped larger mesopores.²⁰

The synthesized ZnO flowers were efficiently tested as an excellent photocatalyst for the self sensitized photodegradation of a cationic triphenylmethane dye, Malachite Green (MG), under solar light. The amount of degradation of MG was almost 94% of the initial dye concentration of 0.2 g L⁻¹ and the initial catalyst amount was 0.02 g in 100 mL solution as shown in Fig. 3.

The possible reason for its excellent photocatalytic activity may be the high surface oxygen vacancies in the ZnO flower confirmed from its room temperature photoluminescence spectra. These high surface oxygen vacancies may allow it to adsorb more O₂ from the water resulting in the formation of a greater number of reactive radicals like O₂^{·-}, OH[·] which contribute to its excellent photocatalytic activity.

Photodegradation of the dye leads to complete mineralization under solar light which was confirmed by qualitatively measuring the CO₂ production using Warburg apparatus. The Warburg manometric method is generally used for biological samples to measure gas absorption as well as gas production.²¹ We took 4 mL of 0.2 g L⁻¹ MG dye and 0.002 g catalyst initially for the experiment. The evolved gas was confirmed to be CO₂ as a BaCO₃ precipitate was formed by adding BaCl₂ solution to the KOH solution, removed from the centre wells of the Warburg vessels, using CO₂ free water.

In summary, flower shaped homocentric pencil like ZnO nanorod bundles, or ZnO flowers, can be successfully synthesized using PEG-4000 as a template under hydrothermal treatment at a moderate temperature and they exhibit excellent photocatalytic activity for the degradation of environmentally hazardous malachite green dye under solar light irradiation. The photodegradation of malachite green results in the complete mineralization of dye to produce CO₂ instead of producing more hazardous aromatic compounds. This ZnO

material may also be applied for the degradation of other hazardous dyes found in industrial waste and dye contaminated water. Further modifications, like doping noble metals, which may improve its photocatalytic activity, require further research.

We would like to thank the Department of Science and Technology, New Delhi for the financial support (GPP-0267). We are also grateful to Dr R. C. Boruah, Acting Director, Dr D. K. Dutta, Chief Scientist, Dr Pinaki Sengupta, Head and Chief Scientist, Materials Science Division and Mr Ananta Kr Sarma, Biotechnology Division, CSIR-North East Institute of Science and Technology, Jorhat for their support.

Notes and references

- (a) Z. W. Dong, C. F. Zhang, H. Deng, G. J. You and S. X. Qian, *Mater. Chem. Phys.*, 2006, **99**, 160–163; (b) W.-N. Li, J. Yuan, X.-F. Shen, S. G. Mower, L.-P. Xu, S. Sithambaram, M. Aindow and S. L. Suib, *Adv. Funct. Mater.*, 2006, **16**, 1247–1253; (c) L. Xu, Y.-S. Ding, C.-H. Chen, L. Zhao, C. Rimkus, R. Joesten and S. L. Suib, *Chem. Mater.*, 2008, **20**, 308–316; (d) R. Mohan, K. Krishnamoorthy and S.-J. Kim, *Solid State Commun.*, 2012, **152**, 375–380.
- (a) J. Goldberger, D. J. Sirbully, M. Law and P. Yang, *J. Phys. Chem. B*, 2005, **109**, 9–14; (b) S. S. Hullavarad, N. V. Hullavarad, P. C. Karulkar, A. Luykx and P. Valdivia, *Nanoscale Res. Lett.*, 2007, **2**, 161–167; (c) X. Wang, J. Liu, J. Song and Z. L. Wang, *Nano Lett.*, 2007, **7**, 2475–2479.
- (a) M. H. Huang, S. Mao, H. Feick, H. Yan, Y. Wu, H. Kind, H. Weber, R. Russo and P. Yang, *Science*, 2001, **292**, 1897–1899; (b) H. Kind, H. Yan, B. Messer, M. Law and P. Yang, *Adv. Mater.*, 2002, **14**, 158–160; (c) M. Zamfirescu, A. Kavokin, B. Gil, G. Malpuech and M. Kaliteevski, *Phys. Rev. B: Condens. Matter*, 2002, **65**, 161205.
- (a) Y. W. Zhu, H. Z. Zhang, X. C. Sun, S. Q. Feng, J. Xu, Q. Zhao, B. Xiang, R. M. Wang and D. P. Yu, *Appl. Phys. Lett.*, 2003, **83**, 144; (b) J. Song, S. A. Kulinich, J. Yan, Z. Li, J. He, C. Kan and H. Zeng, *Adv. Mater.*, 2013, **25**, 5750–5755; (c) H. Zeng, X. Xu, Y. Bando, U. K. Gautam, T. Zhai, X. Fang, B. Liu and D. Golberg, *Adv. Funct. Mater.*, 2009, **19**, 3165–3172.
- Q. H. Li, Y. X. Liang, Q. Wan and T. H. Wang, *Appl. Phys. Lett.*, 2004, **85**, 6389.
- (a) E. C. Greyson, Y. Babayan and T. W. Odom, *Adv. Mater.*, 2004, **16**, 1348–1352; (b) R. Mohan, K. Krishnamoorthy and S.-J. Kim, *Chem. Phys. Lett.*, 2012, **539–540**, 83–88.
- Y. Sun, G. M. Fuge, N. A. Fox, D. J. Riley and M. N. R. Ashfold, *Adv. Mater.*, 2005, **17**, 2477–2481.
- Z. X. Pan, Z. R. Dai and Z. L. Wang, *Science*, 2001, **291**, 1947–1949.
- P. X. Gao and Z. L. Wang, *Appl. Phys. Lett.*, 2004, **84**, 2883.
- P. X. Gao and Z. L. Wang, *J. Am. Chem. Soc.*, 2003, **125**, 11299–11305.
- (a) Y.-J. Choi, J.-H. Park and J.-G. Park, *J. Mater. Res.*, 2005, **20**, 959–964; (b) Y. J. Xing, Z. H. Xi, X. D. Zhang, J. H. Song, R. M. Wang, J. Xu, Z. Q. Xue and D. P. Yu, *Appl. Phys. A*, 2005, **80**, 1527–1530.

- 12 M. J. Zheng, L. D. Zhang, G. H. Li and W. Z. Shen, *Chem. Phys. Lett.*, 2002, **363**, 123–128.
- 13 S. Ohara, T. Mousavand, M. Umetsu, S. Takami, T. Adschiri, Y. Kuroki and M. Takata, *Solid State Ionics*, 2004, **172**, 261–264.
- 14 W. T. Chiou, W. Y. Wu and J. M. Ting, *Diamond Relat. Mater.*, 2003, **12**, 1841–1844.
- 15 J.-H. Park, Y.-J. Choi and J.-G. Park, *J. Cryst. Growth*, 2005, **280**, 161–167.
- 16 X. Y. Kong, Y. Ding, R. Yang and Z. L. Wang, *Science*, 2004, **303**, 1348–1351.
- 17 Z. L. Wang, X. Y. Kong and J. M. Zuo, *Phys. Rev. Lett.*, 2003, **91**, 185502.
- 18 G. Sun, M. Cao, Y. Wang, C. Hu, Y. Liu, L. Ren and Z. Pu, *Mater. Lett.*, 2006, **60**, 2777.
- 19 B. Lin, Z. Fu and Y. Jia, *Appl. Phys. Lett.*, 2001, **79**, 943.
- 20 Z. Xingfu, H. Zhaolin, F. Yiqun, C. Su, D. Weiping and X. Nanping, *J. Phys. Chem. C*, 2008, **112**, 11722–11728.
- 21 R. B. Hespell and E. C. Parola, *J. Bacteriol.*, 1970, **103**, 216–226.